

# Semiclassical statistico-dynamical description of polyatomic photo-dissociations: State-resolved distributions.

Maykel Leonardo González-Martínez,<sup>1,2,\*</sup> Laurent Bonnet,<sup>2,†</sup> Pascal Larrégaray,<sup>2</sup> and Jean-Claude Rayez<sup>2</sup>

<sup>1</sup>*Departamento de Física General, Instituto Superior de Tecnologías y Ciencias Aplicadas, Habana 6163, Cuba*

<sup>2</sup>*Institut des Sciences Moléculaires, Université Bordeaux 1,  
351 Cours de la Libération, 33405 Talence Cedex, France*

(Dated: November 5, 2018)

An alternative methodology to investigate indirect polyatomic processes with quasi-classical trajectories is proposed, which effectively avoids any binning or weighting procedure while provides rovibrational resolution. Initial classical states are started in terms of angle-action variables to closely match the quantum experimental conditions and later transformed into Cartesian coordinates, following an algorithm very recently published [*J. Chem. Phys.* **130**, 114103 (2009)]. Trajectories are then propagated using the ‘association’ picture, *i.e.* an inverse dynamics simulation in the spirit of the exit-channel corrected phase space theory of Hamilton and Brumer [*J. Chem. Phys.* **82**, 595 (1985)], which is shown to be particularly convenient. Finally, an approximate quasi-classical formula is provided which under general conditions can be used to add possible rotational structures into the vibrationally-resolved quasi-classical distributions. To introduce the method and illustrate its capabilities, correlated translational energy distributions from recent experiments in the photo-dissociation of ketene at 308 nm [*J. Chem. Phys.* **124**, 014303 (2006)] are investigated. Quite generally, the overall theoretical algorithm reduces the total number of trajectories to integrate and allows for fully theoretical predictions of experiments on polyatomics.

PACS numbers: 31.15.xg, 34.10.+x, 82.20.Bc, 82.37.Np

## I. INTRODUCTION

The 20th century witnessed both the advent of modern computers and the associated exponential growth in computational power, which continues nowadays. As more can be done in significantly less time, simulation of inherently more complex processes and/or larger systems is attempted. In the field of chemical physics, what started as describing atomic and diatomic molecular processes currently looks after the simulation of, *e.g.* larger polyatomics, clusters, phenomena at surfaces and biomolecular complexes of interest.

However, despite all the effort being devoted to develop approaches which include quantum effects in the dynamics of large molecular systems [1], realistic quantum-mechanical *simulations* of polyatomic processes remain prohibitively expensive. To date, the only general theoretical alternative is the quasi-classical trajectory method (QCT) [2, 3, 4], which is based on numerically solving Hamilton’s (or Newton’s) equations of motion. Primarily, this is due to the cumbersome basis sets that need to be handled within quantum calculations in order to avoid crude approximations, but also partially because developing general, *i.e.* *scalable* classical trajectory codes is relatively easier.

To allow for comparison with experiments, both the selection of classical initial conditions and the statistical treatment of QCT results should be semiclassical in

spirit. In particular, to mimic quantum features using classical (continuous) magnitudes, additional *binning* or *weighting* procedures are quite difficult to avoid. As implied, the underlying source of the problem—as with some other drawbacks of QCT—is that classically, vibrations and rotations are not quantised *per se*. In this regard, important advances have been made in the last few years by replacing the standard/histogram binning (SB) procedure by a Gaussian weighting (GW) [5, 6, 7, 8, 9, 10, 11, 12]. In the latter, the different trajectories are assigned different (Gaussian) statistical weights, larger the closer its final actions to integer values. Despite its many promising capabilities, we have recently pointed out how the convergence of GW could be affected when applied to processes involving polyatomics [11]. This is mainly because increasing the number of atoms in a molecule will almost certainly increase the number of modes for which a quantum–mechanical description is convenient—and Gaussian weights must be assigned. As a result, the overall weight of a given trajectory could be *significantly* reduced, in particular if several actions vary simultaneously.

At the same time, powerful experimental techniques have been developed during the precedent decades and very precise measurements of state-to-state observables are now possible. Correlated product distributions—where final state and/or translational energy distributions are measured in coincidence with given rovibrational states of the products—are among such. These increasingly sophisticated experiments demand finer statistics on the QCT results for highly resolved, intrinsically quantum features are much more difficult to ‘converge’ using classical mechanics. The ‘brute force’ approach

---

\*Corresponding author, E-mail: mleo@instec.cu

†Corresponding author, E-mail: l.bonnet@ism.u-bordeaux1.fr

is of course to increase the number of trajectories in the classical ensemble—and as their propagation is easily task-parallelised, *i.e.* particularly suitable to solve in computer clusters—running millions of such is becoming common.

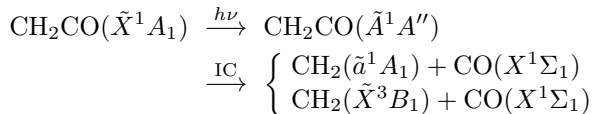
In this work we report on an alternative QCT algorithm for investigating polyatomic processes which effectively avoids any binning or weighting method while provides both vibrational and rotational resolution. Its main advantage comes from the fact that initial conditions are directly generated at the semiclassical rovibrational states of interest in terms of angle-action variables, which automatically reduces the total number of trajectories to integrate. These are however propagated in Cartesian coordinates, by means of a transformation very recently published [13]. In addition, a quasi-classical formula is derived to further incorporate possible rotational structures. To introduce and illustrate the capabilities of our method, we simulate highly-structured empirical correlated product distributions from the dissociation of ketene at 308 nm [14].

The paper is organized as follows: the problem, theoretical aspects of the QCT implementation and results of its application are dealt with in Section II and later discussed in Section III; at last, Section IV summarizes.

## II. THEORY AND APPLICATION

### A. Ketene dissociation at the $S_0$ electronic surface

The photo-fragmentation of ketene,



is arguably the most intensively investigated polyatomic process in the last decades, *cf.* [14, 15, 16, 17, 18, 19, 20, 21, 22, 23, 24, 25, 26, 27, 28, 29, 30, 31, 32, 33, 34]. At present, it is firmly established that following optical excitation to the  $\tilde{A}^1A''$  state, the molecule either undergoes intersystem crossing to the lowest-lying, triplet, or fast internal conversion to the singlet electronic state. From these, dissociation into methylene and carbon monoxide occurs. Despite the triplet threshold lies  $\sim 3150 \text{ cm}^{-1}$  below the singlet, the fact that it presents a (small) barrier to dissociation—of a few cents of inverse centimetres—, but mainly, that the interaction which accounts for the change in electronic spin is rather weak, makes the singlet channel statistically dominant from excess energies as low as  $100\text{--}200 \text{ cm}^{-1}$ . Such conditions make this process an effective prototype for a *barrierless polyatomic* unimolecular reaction on a *single* potential energy surface (PES). Experimentally, it has the additional advantage of a well-defined total energy and time origin distinctive of photo-dissociations [14].

Earlier measurements of energy-dependent rates and overall product distributions were used as benchmarks to test and develop various statistical models including phase space theory (PST) and Rice–Ramsperger–Kassel–Marcus (RRKM) theory, *cf.* [21, 22, 23, 24]. It was concluded that under moderate excitations the molecule dissociates statistically, exit-channel effects becoming increasingly important with augmenting energy. The dissociating picture therefore evolves from that of a loose to a tight transition state (TS) [31]. During the last decade, however, there has been growing interest in the problem of correlated product distributions [14, 27, 32]. In the most recent experiments, Komissarov *et al.* [14] studied the photo-fragmentation of the molecule at 308 nm and measured product translational energy distributions for specific rotational states of CO, *i.e.*  $P(E_t; j_{\text{CO}})$ . These are the observables we will focus on in the present work.

### B. Singlet potential energy surface

Extensive trajectory calculations require a reliable numerical representation of the singlet PES. This was generated from the most recently reported high-level *ab initio* data [29]. In this work, Klippenstein, East and Allen used a separation in transitional and conserved modes to determine the quadratic force fields along the reaction path—at the CCSD/[5s4p2d, 4s2p] level of theory—in terms of  $C_s^I$  symmetry internal coordinates. For excess energies of the order of that obtained with a 308 nm laser ( $E_{\text{exc}} \approx 2350 \text{ cm}^{-1}$ ), these force fields should provide all essential information on the couplings between the intra-fragment modes and the dissociation coordinate in the vicinity of the reaction path, as well as the interaction dependence on the mutual orientation of the fragments<sup>1</sup>. To further assess its quality, in the same work, the authors showed that variational RRKM energy-dependent rates predicted with this PES are in quantitative agreement with the experiment.

Being  $\mathbf{S} = \{S_i\}$  the symmetry internal coordinates,  $F_{ij}$  ( $i, j = \overline{1, 9}$ ) the quadratic force constants and  $V_{\text{CC}}$  (Fig. 7 in Ref. [29]) the minimum potential energy along the reaction path as a function of the C–C interatomic distance,  $S_4$ , the PES may be written as

$$V(\mathbf{S}) = V_{\text{CC}}(S_4) + \frac{1}{2} \sum_{i=1}^9 \sum_{\substack{j=1 \\ j \neq 4}}^9 F_{ij} (S_i - S_{0i})(S_j - S_{0j}), \quad (1)$$

where most  $S_{0k} = S_{0k}(S_4)$  can be straightforwardly calculated from the definitions of symmetry internal coordinates and the analytic parametrizations for the reaction path (Tables VI and III, *ibid.*). The slightly

<sup>1</sup> We discuss the implications of this quadratic approximation to the PES for trajectory calculations in some detail in Section II C 5.

more elaborate are  $S_{06} = \sqrt{2} \arccos[-\cos(\alpha/2) \cos \gamma]$  and  $S_{09} = \sqrt{2} \arccos[-\cos(\alpha/2) \sin \gamma \sin^{-1} \beta]$ , where— if individual ketene atoms are numbered as they enter in the chemical formula— $\alpha = \angle(\text{H}^1\text{C}^1\text{H}^2)$ ,  $\beta = \beta_{1,2} = \angle(\text{H}^1,^2\text{C}^1\text{C}^2)$  and  $\gamma$  ( $\text{CH}_2$  wagging angle) are all angular internal coordinates defined in Fig. 1 of the same work. The  $F_{ij}$  functions were obtained from fittings to values in Table VI, *ibid.*

Finally, we validated the PES by diagonalising the Hessian matrix and confirming that all local harmonic frequencies previously reported (Table VII in Ref. [29]) were successfully reproduced.

### C. Quasi-classical trajectories

We will introduce in what follows a particular implementation of QCT ideas and show its predictive power in the simulation of highly-resolved  $j_{\text{CO}}$ -correlated translational energy distributions, from the unimolecular dissociation of ketene. Theoretically, it can be assumed that under the experimental conditions reported in Ref. [14], these product distributions correspond to a given total energy  $E = E_{\text{exc}} + E_{\text{nmodes}}$  and angular momenta  $J$ , *i.e.*  $P(E_{\text{t}}; j_{\text{CO}}) \equiv P(E_{\text{t}}; E, J, j_{\text{CO}})$ . The zero-point energy in the molecule normal modes,  $E_{\text{nmodes}} \approx 4730 \text{ cm}^{-1}$ .

In reading the following section, it is important to keep in mind that we use an association rather than a dissociation picture for propagating trajectories. This is based on a method due to Hamilton and Brumer [35] which will be introduced in Section II C 2, where its many advantages are also discussed.

#### 1. Initial conditions: Angle-action variables and the transformation to Cartesian coordinates

Within QCT, it is always preferred to generate the ensemble of classical initial conditions for the very precise quantum states explored in the experiment. Such a generation is *naturally* performed in terms of angle-action variables [36, 37, 38, 39], the actions being the classical counterpart of quantum numbers<sup>2</sup>. These variables, however, should preferably not be used to run trajectories for they may lead to strong numerical instabilities. In fact, Cartesian coordinates are ideal to solve the classical equations of motion for molecular processes involving polyatomics. Codes built on these coordinates should result easily scalable and standard numerical approaches, adequate. Therefore, the transformation from angle-action variables to Cartesian coordinates is an important step in QCT. Very recently, we reported on such a transformation [13] that fits to our purposes here.

Discarding all center-of-mass coordinates the phase-space results

$$\Gamma = \{R, q_i, \alpha, \beta, \alpha_l, \alpha_1, \alpha_2, \alpha_k, \gamma_1\} \\ \otimes \{P, x_i, J, J_z, l, j_1, j_2, k, \kappa_1\}; i = \overline{1, 4}, \quad (2)$$

where  $R$  and  $P$  are the dissociation coordinate—the  $\text{CH}_2$  and  $\text{CO}$  fragments centres-of-mass relative distance—and conjugate momentum. The remaining 22 angle-action variables are [13]:  $q_i, x_i$ , the vibrational phase and corresponding action of the  $i$ th normal mode of  $\text{CH}_2$  ( $i = \overline{1, 3}$ ) and  $\text{CO}$  ( $i = 4$ );  $J, J_z$ , the moduli of the total angular momentum and its  $z$ -axis projection in the laboratory frame;  $l$ , the modulus of the orbital angular momentum;  $j_1, j_2$ , the moduli of  $\text{CH}_2$  and  $\text{CO}$  rotational angular momenta;  $k$ , the modulus of the total rotational angular momentum  $\mathbf{k} = \mathbf{j}_1 + \mathbf{j}_2$ ; and  $\kappa_1$ , the algebraic value of the projection of  $\mathbf{j}_1$  onto the  $C_2$  axis of  $\text{CH}_2$ . Finally,  $\alpha, \beta, \alpha_l, \alpha_1, \alpha_2, \alpha_k$  and  $\gamma_1$  are respectively all the angles conjugate to the angular momenta mentioned above. It is apparent that in terms of these variables we can effectively set up, individually, *all* the vibrational *and* rotational modes of the fragments.

Given  $E, J$  (fixed to 1) and  $j_2$  ( $\equiv j_{\text{CO}}$ )—for each set of energetically permitted vibrational states  $x_i, i = \overline{1, 4}$ —the total available energy  $E_{\text{avail}}$  and maximum allowed values  $l_{\text{max}}$  and  $j_{1,\text{max}}$  are completely determined<sup>3</sup>. From all these,  $J_z, k$  and  $\kappa_1$  are thus randomly selected from uniform distributions according to  $J_z \in [-J, J], |j_{1,\text{max}} - j_2| \leq k \leq j_{1,\text{max}} + j_2$  and  $\kappa_1 \in [-j_{1,\text{max}}, j_{1,\text{max}}]$ . Microcanonical distributions are finally obtained by aleatory selection of all angles and phases from a uniform distribution in  $[0, 2\pi]$ . All vector constraints on the set of angular momenta must also be satisfied.

At this point, the  $\Gamma$  vector is transformed to Cartesian coordinates, using the algorithm presented in Ref. [13]. Here, a slight readjustment is necessary due to the conditions of the experiment, as the *total energy* of the system—rather than the relative velocity between the fragments—must be *fixed*. Specifically, the three Cartesian components of  $\mathbf{P}$  (Section II C 3 in Ref. [13]) should be computed right before the final step (determination of nuclear momenta, second part of Section II C 11, *ibid.*) for only at this point it is possible to calculate the energy available to translation,  $E_{\text{avail,t}}$ , from which  $P = \sqrt{2\mu E_{\text{avail,t}}}$  ( $\mu$  being the system reduced mass). Computationally, an incubation period is needed before using an otherwise acceptable initial state to avoid possible correlations in the numerical generation of pseudo-random numbers.

<sup>2</sup> Throughout this work all actions will be quoted in  $\hbar$  units.

<sup>3</sup> The choice of  $R$  will become apparent in Sections II C 2 and II C 3.

## 2. Propagation: Exit-channel corrected phase space theory

As previously seen (Section II A), it is possible to assume that the photo-excited ketene forms a long-lived intermediate complex prior to fragmentation, which justifies the use of a microcanonical distribution at the TS. In this work, extensive trajectory calculations were performed in conformity to the so-called exit-channel corrected phase space theory (ECCPST), proposed in the 1980s by Hamilton and Brumer [35]. Within this method, a microcanonical set of trajectories are initiated in the products and directed towards the unimolecule region, the statistics being performed with those ‘successful’ trajectories reaching the TS. Clearly, the underlying assumption here is that the time-reversed dynamics of this subset of trajectories yields a microcanonical distribution at the TS [35]. The method bears certain similarities with the statistical quasi-classical trajectory (SQCT) model for atom-diatom insertion reactions of Aoiz and co-workers [40].

Besides its simplicity, the ECCPST offers quite a few practical advantages, *e.g.* (1) initial conditions are generated where the assumptions for partitioning into product normal modes are best fulfilled—*i.e.* at the interfragment distance for which the interaction between the CH<sub>2</sub> and CO is negligible—so the usual dispersion in the ensemble’s total energy will be minimum (of about 2–3 cm<sup>-1</sup> in our calculations); (2) all threshold behaviour is expected to be reproduced at its best, since product states are given precise energies in direct correspondence to their quantum counterparts; (3) initial conditions are straightforwardly defined by fixing the centres-of-mass distance between the resulting fragments—which explicitly appears in the transformation from angle-action variables to Cartesian coordinates [13]—while the TS can be re-defined at convenience during propagation (in this case, by the C–C interatomic distance which was proven best [29]); (4) since product states statistics is performed on a subset of initial conditions, the extra (non-trivial) work of discretising classical magnitudes at the end of the trajectories is avoided; (5) any binning or weighting to cope with the conceivable non-adiabaticity of vibrations in the course of reaction—which was found to be of about 15–20% after some preliminary calculations—can be avoided; and (6) the PES does not need to be determined within the reactant region. A few other advantages will be discussed in the following sections.

The main drawback, however, is that (possibly) many trajectories are propagated which never actually reach the TS. In fact, we found that approximately only 1 out of 10 trajectories enters the reactants region<sup>4</sup>. The overall

<sup>4</sup> The indetermination on the exact TS location makes necessary to discard some trajectories even when propagating outwards from the reactants region. In this case, these constitute nearly one half of the total ensemble.

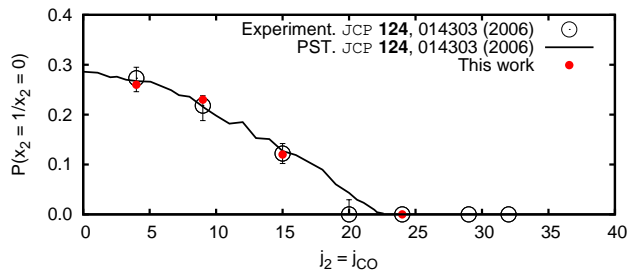


FIG. 1: (Colour online) Vibrational branching ratio for singlet CH<sub>2</sub> in coincidence with selected CO( $x_4 = 0$ ,  $j_2$ ) states. Comparison with experimental and previous PST calculations.

propagation time may thus be significantly reduced by applying strategies to quickly identify those trajectories which will ultimately be discarded.

## 3. Computational details: integration and convergence

Except when stated contrary, batches of  $5 \times 10^4$  trajectories were started at  $R^\infty = 10 \text{ \AA}$  and propagated towards the unimolecule region in accordance with ECCPST (Section II C 2). Convergence of reported product translational energy distributions was tested by confirming that those obtained with  $2 \times 10^5$  trajectories are statistically identical.

A fixed-step fourth-order Adams-Bashforth-Moulton predictor-corrector method initialised with a fourth-order Runge-Kutta integrator was used for propagation. Trajectories were followed until one of two conditions was fulfilled: (1) the molecule reached the transition state (at the C–C interatomic distance  $R^\ddagger \equiv R_{CC}$ , as relevant to the specific excitation energy from Table X in Ref. [29]); and (2)  $t = T_{\max} = 20 \text{ ps}$ . The step size  $\Delta t = 2 \times 10^{-4} \text{ ps}$  was adjusted so that the maximum error in total energy did not exceed  $\Delta E = 20 \text{ cm}^{-1}$ , *i.e.* less than 0.3% of  $E$ , with which the mean error was  $\langle \Delta E \rangle = 5 \text{ cm}^{-1}$ . Under these conditions, the fraction of non-fragmented to fragmented trajectories was consistently smaller than 0.5%. Typically, a single trajectory required between 1 and 3 seconds of CPU time—according to the specific values of  $x_2$  and  $j_2$ —on an Altix XE210 computer with two Dual-Core Intel<sup>®</sup> Xeon<sup>®</sup> 5030 (‘Dempsey’) processors.

## 4. Correlated translational energy distributions

After the subset of trajectories reaching the TS is identified, the  $P^C(E_t; E, J, x_2, j_{CO})$  distribution corresponding to each  $x_2$  scissor mode of CH<sub>2</sub> is calculated by standard statistics over it. From these, the overall correlated translational energy distribution  $P^C(E_t; E, J, j_{CO})$  is obtained by merging the different  $x_2$  contributions altogether, with the corresponding weights according to the vibrational branching ratios shown in Fig. 1.

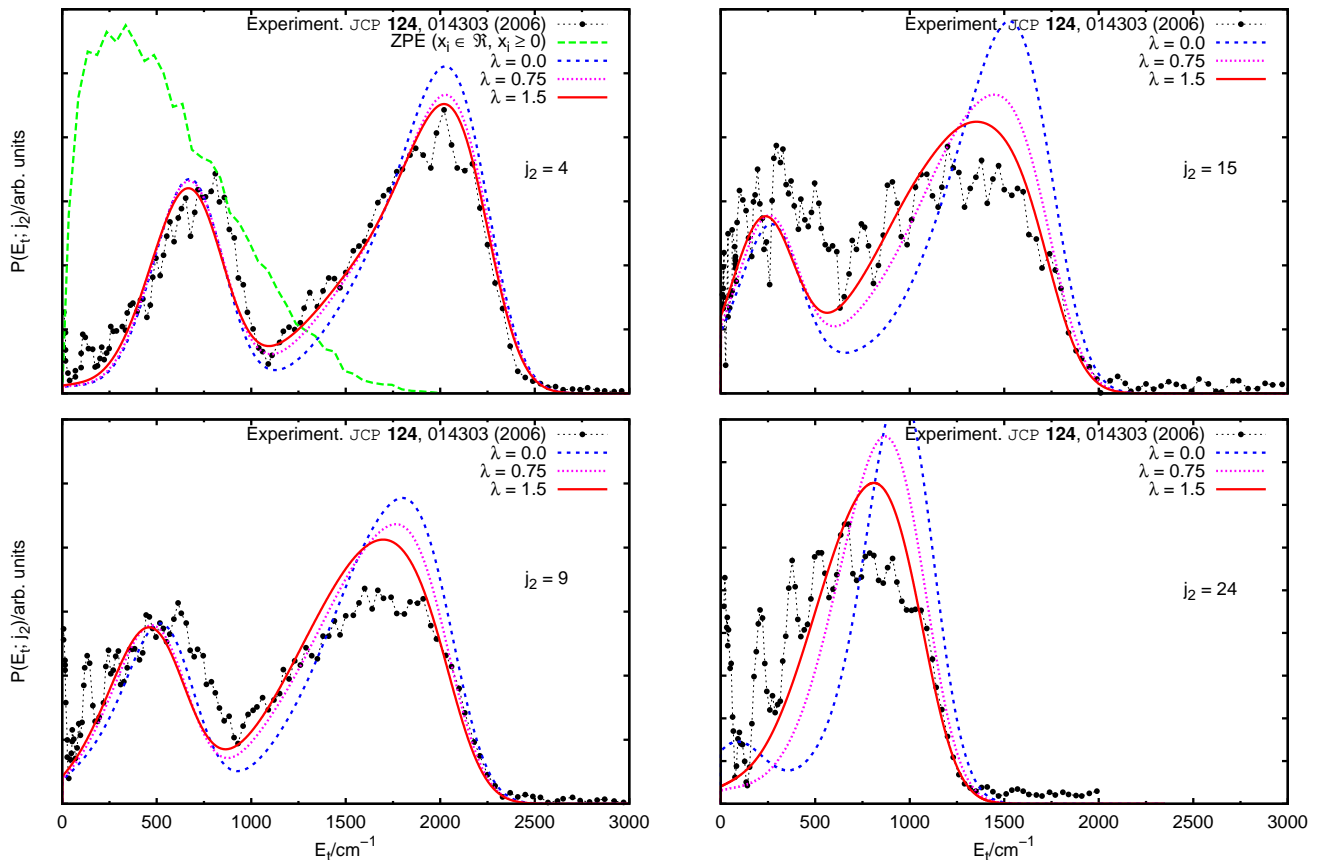


FIG. 2: (Colour online) Correlated product translational energy distributions after excitation with a 308 nm laser: QCT results with vibrational resolution. Comparison with the experiment.

In principle, to predict these weights at a given  $j_2$  state of interest two contributions need to be taken into account. First, Monte Carlo methods should be applied to find the relative probability that for each scissor state  $x_2$  a given set of angle-action variables is finally accepted as a valid initial condition. Here the ECCPST proves again particularly convenient, since this is readily done if track is kept on the percent of successful trials and the hypervolume in phase space from which each  $x_2$  set of initial conditions was randomly selected. The second step is to correct this relative probability for dynamical effects, which in practice would mean to determine the ratio of capture probabilities from each scissor mode. Despite its apparent simplicity, obtaining a reliable approximation for the latter could be difficult for it not only depends on the quality of the PES, but also on the relative accuracy of TS locations and the set of integration parameters. However, it was previously shown that, by cancellation of errors, *least-biased* values (also referred as PST, depending on the convention employed) are in excellent agreement with the experiment [14]. The values reported in Fig. 1 are directly calculated from our initial conditions by the algorithm explained at the top of this paragraph. Their agreement with experimental

and previous theoretical values confirms the correctness of our approach. At last, the theoretical distributions are Gaussian-blurred to match the experimental resolution.

Calculated curves for several representative  $j_2$  states are compared with measurements in Fig. 2—and have been quoted as ‘ $\lambda = 0.0$ ’ (blue), the reason for which will be given in the following section. The reported contributions from adjacent rotational states [14] was appropriately taken into account to produce the distributions corresponding to  $j_2 = 4$  and 9. Additionally, the zero-point-energy (ZPE) corrected distribution [41] has been included in the  $j_2 = 4$  panel, which illustrates the general behaviour for all other rotational states. To produce the latter, an ensemble of  $2 \times 10^5$  initial conditions with continuous actions was started in the products, being the vibrational modes constraint between zero and their maximum energetically allowed values.

### 5. A modification to the PES

Except of course for the  $j_2 = 24$  rotational state, all ‘ $\lambda = 0.0$ ’ theoretical curves in Fig. 2 have the correct bimodal shape due to the excitation of the first and

the ground states of methylene’s scissor mode (with frequency  $w_2 \approx 1400 \text{ cm}^{-1}$ ). The experimental positions of the peaks are also fairly well reproduced. It is important to stress here that neither of these facts is trivial. Note, for example, the strong discrepancy of the ZPE-corrected curve which fails to reproduce any of them. Moreover, to achieve a similar agreement with the experiment in the case of the triatomic dissociation  $\text{NCO} \rightarrow \text{N} + \text{CO}$ , the GM method had to be applied [9]. However, the divergence between the experimental and ZPE distributions has an additional important implication. As the population corresponding to the ground state of the  $\text{CH}_2$  scissor mode  $x_2 = 0$  is practically negligible, even by using the GW one could never obtain the proper translational energy distributions from ZPE-corrected calculations only. It is thus crucial that, at this point, the ‘vibrational’ resolution has been naturally obtained within QCT and no binning or weighting procedure is needed.

However, it is clear that within each vibrational lobe, these theoretical distributions tend to predict larger than observed populations of low  $\text{CH}_2$  rotational levels. A plausible explanation may be derived from calculations on triatomic complexes. From these, it is known that quadratic representations of PES systematically tend to overestimate the energy transfers from the diatomic rotation to the inter-fragment translational degree of freedom [42]. Physically, this is due to the bending mode being unrealistically hindered, *i.e.* insufficiently damped, in the course of fragmentation.

The previous reaction rate calculations on this PES [29], being an observable of ‘global’ character, would very likely not depend as strongly as the distributions we intend to reproduce. Nevertheless, only the construction of a new global PES or *ab initio* dynamics calculations could give a reliable answer to this issue. Both these are beyond the scope of the present work.

On the other hand, several modifications can be attempted in order to bring the rotation-to-translation transfers closer to the empirical observations, under various physical grounds. One possible direction is to slightly change the force constants related with the molecular modes directly responsible for such transfers. The alternative followed here was to rewrite the PES as

$$V_\lambda(\mathbf{S}) = xV(\mathbf{S}) + (1-x)V^\infty(\mathbf{S}), \quad (3)$$

where  $x = \exp[-\lambda(S_4 - R^\ddagger)]$  and  $V^\infty = V_{\text{CH}_2} + V_{\text{CO}}$  is simply the asymptotic potential interaction. Eq. (3) conserves both the PES at the TS and the correct asymptotic behaviour. In particular,  $\lambda = 0$  corresponds to the original PES. Physically sensible values for the damping parameter  $\lambda$ , from calculations on triatomic systems, are usually between 2 and 3.

Trajectories were propagated on the modified PES of Eq. (3) and the theoretical curves corresponding to  $\lambda = 0.75$  and 1.5 are included in Fig. 2. From these, it is clear that reducing the energy transfer between  $\text{CH}_2$  rotation and inter-fragment recoil translation invariably leads to the overall experimental trend. The change is

more strongly pronounced at higher CO rotational excitations and all  $\lambda = 1.5$  curves are in very good agreement with the experiment.

#### D. ‘Inserting’ the $\text{CH}_2$ rotational structure

From Fig. 2 is readily seen that the main qualitative difference between ours (*e.g.*,  $\lambda = 1.5$ ) and the experimental results is the rotational structure observed in the latter, which relates to that of  $\text{CH}_2(\tilde{a}^1A_1)$ . In this section we show how these features can also be theoretically reproduced by the adequate modification of the  $P^C(E_t; E, J, j_{\text{CO}})$  distributions.

##### 1. A quasi-classical formula to get the rotational resolution

Let us first consider the simpler though instructive case of a triatomic unimolecular dissociation  $\text{ABC} \rightarrow \text{A} + \text{BC}(v, j)$ , at fixed total energy  $E$  and angular momentum  $J$ . Here,  $v, j$  represent the vibrational and rotational states of the diatomic fragment. In particular, we are interested in the vibrationally-resolved product translational energy distribution (at a sufficiently large value of the inter-fragment distance  $R^\infty$ ).

Classically, after removing all center-of-mass coordinates, this is exactly

$$P^C(E_t; E, J, v) = \int_{\Gamma} \prod_{i=1}^5 \Delta_i \chi(\Gamma) d\Gamma, \quad (4)$$

being

$$\Gamma = \{R, q, \alpha, \beta, \alpha_l, \alpha_j, P, x, J', J_z, l, j\} \quad (5)$$

the physically relevant set of angle-action variables (complemented with the dissociation coordinate  $R$  and its conjugate momentum  $P$ , *e.g.* Eq. (2)), and

$$\Delta_1 = \delta(\mathcal{H}_t - E_t), \quad (6)$$

$$\Delta_2 = \delta(\mathcal{H} - E), \quad (7)$$

$$\Delta_3 = \delta(J' - J), \quad (8)$$

$$\Delta_4 = \delta(x - v), \quad (9)$$

$$\Delta_5 = \frac{P}{\mu} \Theta(P) \delta(R - R^\infty), \quad (10)$$

where  $\Delta_1$  to  $\Delta_4$  explicitly account for all fixed magnitudes while  $\Delta_5$  limits integration to the *outgoing flux* through the  $R = R^\infty$  surface. As usual,  $\delta$  and  $\Theta$  are respectively Dirac’s  $\delta$ - and Heaviside functions. In addition, the total Hamilton function has been partitioned as  $\mathcal{H} = \mathcal{H}_t + \mathcal{H}_{\text{rv}}$ , *i.e.* into its translational and rovibrational components, with

$$\mathcal{H}_t = \frac{1}{2\mu} \left( P^2 + \frac{l^2}{R^2} \right) + V_{\text{A,BC}}. \quad (11)$$

By definition, the interaction potential of A with respect to BC,  $V_{A,BC}$ , tends to zero as  $R \rightarrow R^\infty$ .

At last,  $\chi(\mathbf{\Gamma})d\mathbf{\Gamma}$  is the probability for the system mechanical state to be in the volume  $\mathbf{\Gamma}$  of phase space. The  $\chi(\mathbf{\Gamma})$  function can be rewritten as

$$\chi(\mathbf{\Gamma}) = C_{JJ_zlj}\tilde{\chi}(\mathbf{\Gamma}), \quad (12)$$

where  $C_{JJ_zlj} = \Delta(J, l, j)\Theta(J - |J_z|)$  holds all vector constraints,  $\Delta$  representing a triangular inequality.  $\tilde{\chi}$  is effectively independent of  $R^\infty$  (provided this is large enough) and carries *all* the information on the full dissociation process: that coming from both the initial state distribution and possible *dynamical effects*, *i.e.* the state-to-state transition probabilities.

On recalling some basic  $\delta$ -function properties, partial integration in Eq. (4) can be shown to yield (we simplify notation by discarding the explicit parametric dependence with respect to  $E$  and  $J$  in what follows)

$$P^C(E_t; v) \propto \int C_{JJ_zlj}\delta(E - E_t - E_{rv}) \times \bar{\chi}(E_t, J_z, l, j; v) dJ_z dl dj, \quad (13)$$

where  $E_{rv}$  is the rovibrational energy of BC and  $\bar{\chi}$  is the angle/phase average of  $\tilde{\chi}$ . The centrifugal orbital term has been neglected for it depends on  $R^{-2}$  which becomes negligible as  $R \rightarrow R^\infty$ . Using the mean value theorem, this can be expressed as

$$P^C(E_t; v) = \Xi^C(E_t; v)P_{LB}^C(E_t; v), \quad (14)$$

being

$$P_{LB}^C(E_t; v) = \int C_{JJ_zlj}\delta(E - E_t - E_{rv})dJ_z dl dj \quad (15)$$

the (classical) *least-biased* vibrationally-resolved product translational energy distribution.

Eq. (14) may even look deceptively simple, though its derivation here proves useful to disentangle the physical origin of its factors. In a sense, the underlying ideas can be related to the theory of surprisal analysis of Levine and Bernstein [43], if the least-biased plays the role of the prior distribution. Eq. (14) basically states that  $P^C$  differs by a scaling factor (which in turn depends on  $E_t$  and  $v$ ) with respect to the least-biased value  $P_{LB}^C$ . The factor itself,  $\Xi^C$ , ‘inherits’ from  $\tilde{\chi}$  all the dynamical information on the particular process, but it is additionally ‘weighted’ by the density of *constraint* rotational states.

In obtaining a quasi-classical analogue to Eq. (14) two approximations are made. First, we replace the integrals in Eq. (15) by the corresponding quantum sums and second, we *postulate* that if QCT founding ideas are valid for the process under study, using  $\Xi^C$  in the place of its quantum analogue  $\Xi^Q$  must be a fairly good approximation. We should note that the latter is not only a dynamical statement, but also a subtle assumption on the equivalence between the classical and convoluted-quantum density of rotational states, which is expected to hold under

quite general conditions<sup>5</sup>. By means of these approximations one can write

$$P^{QC}(E_t; v) = \Xi^C(E_t; v)P_{LB}^Q(E_t; v), \quad (16)$$

which explicitly reads

$$P^{QC}(E_t) = \sum_{\forall v, J_z, l, j} \frac{P^C(E_t; v)}{P_{LB}^C(E_t; v)} C_{JJ_zlj}\delta(E - E_t - E_{rv}), \quad (17)$$

after summing over all possible final vibrational states.

Although our derivation has been made for a triatomic system, it is easy to write the equivalent of Eq. (17) for the correlated translational energy distribution in the fragmentation of ketene

$$P^{QC}(E_t; j_2) = \sum_{\forall v_i, J_z, l, k, j_1, \tau} \frac{P^C(E_t; v_i, j_2)}{P_{LB}^C(E_t; v_i, j_2)} C_{JJ_zlkj_1j_2\tau} \times \delta(E - E_t - E_{rv}), \quad (18)$$

where

$$C_{JJ_zlkj_1j_2\tau} = \Delta(J, l, k)\Delta(k, j_1, j_2)\Theta(J - |J_z|) \times \Theta(j_1 - |\tau|). \quad (19)$$

that finally allows to insert the CH<sub>2</sub> rotational structure to our vibrationally-resolved distributions in Fig. 2. Here  $j_1$  and  $\tau$  constitute mere *labels* for the CH<sub>2</sub> rotational energy levels, as will become apparent in Section IID 2.

The ECCPST proves again particularly convenient as the  $P_{LB}^C$  distribution in Eq. (18) can be directly obtained from the ensemble of microcanonical initial conditions.

## 2. CH<sub>2</sub>( $\tilde{a}^1A_1$ ) asymmetric rotor energy levels

Methylene has different its three principal moments of inertia (*i.e.*  $I_{aa} < I_{bb} < I_{cc}$ ), being thus an asymmetric rotor (AR). There is no general quantum formula which determines the rotational energy levels for such molecules in terms of the set of (quantum numbers) action variables,  $j_1, \kappa_1$ , used for computing the corresponding initial conditions [13].

However, it can be proved that the rigid-rotor Hamiltonian  $\hat{H}_{\text{rot}}$  becomes block-diagonal in the matrix representation of symmetric rotor (SR) eigenfunctions [44, 45]. It is also possible to show that for a given angular momentum  $J$ , every AR state correlates with one prolate ( $J, K_a$ ) and one oblate ( $J, K_c$ ) SR level only. It is thus a very common practice to *label* the AR levels as  $J_{K_a K_c}$ , the indexes taking the values  $K_a \in \{0, 1, 1, 2, 2, \dots, J, J\}$  and  $K_c \in \{J, J, \dots, 2, 2, 1, 1, 0\}$  with increasing energy of the terms. As it is easily seen, one could alternatively

<sup>5</sup> This is not generally true for *vibrational* states, hence we deal with vibrationally-resolved distributions.



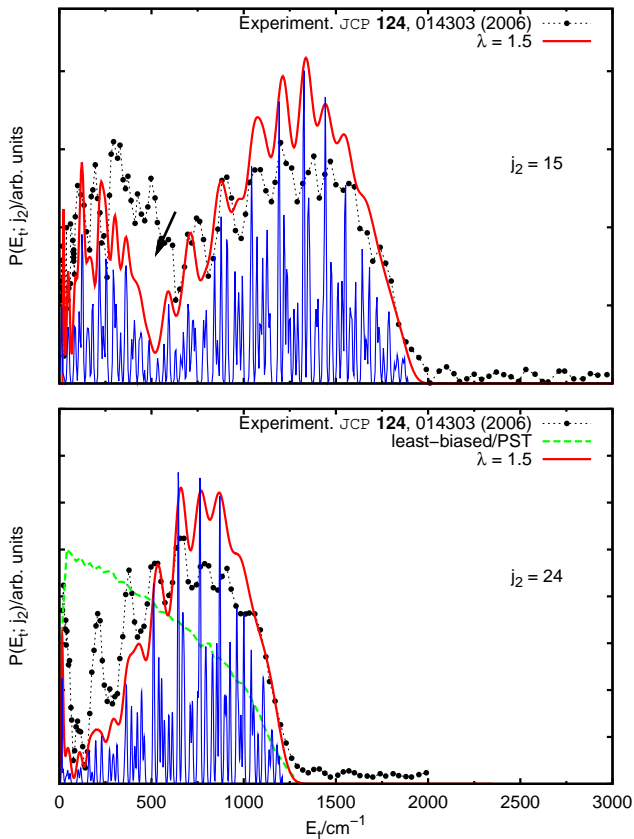


FIG. 3: (Colour online) Correlated product translational energy distributions after excitation with a 308 nm laser: QCT results with rovibrational resolution. Comparison with the experiment.

use a single label defined by  $\tau = K_a - K_c$ , which in turn spans the  $2J + 1$  values from  $-J$  to  $J$ .  $\tau$  rather than  $\kappa_1$  has been used in Eq. (18) to stress the fact that this label has no direct correspondence to the  $\kappa_1$  action.

In our calculations, spectroscopic  $\text{CH}_2(\tilde{a}^1A_1)$  energy levels were used when available and complemented with theoretical AR calculations at higher energies [46, 47]. The error in theoretical values could be of several inverse centimetres, especially at large values of  $j_1$  and  $\tau$ .

### III. DISCUSSION

Rotational structures are barely visible in the measurements for  $j_2 = 4$  and 9, being strongly blurred due to the contribution of adjacent rotational states. Fig. 3 then shows the application of Eq. (18) to  $\lambda = 1.5$  theoretical distributions, corresponding to  $j_2 = 15$  and 24, as a test on the capabilities of the method. Within each panel, two theoretical curves correspond to convolutions with different strengths. One of them (darker, red) has been chosen to closely match the experimental resolution [14] while the other (blue) shows the typical fine structures

which are attainable with our method.

The empirical rotational structure is fairly well reproduced by the QCT calculations, being all theoretical and experimental peaks correctly aligned. The larger disagreement is observed within the upper panel, in the region shown by an arrow. This area corresponds to the matching between the low energy tail of the  $x_2 = 0$  state and the high energy component of  $x_2 = 1$ , being the former the main contribution to it. The discrepancy between our curve and the experiment is thus a secondary effect due to the overestimation of rotation-to-translation transfers already discussed in Section II C 5. It cannot be seen in Fig. 2 as the convolution used there artificially ‘populates’ the missing rotational states.

The least-biased distribution corresponding to  $j_2 = 24$  is also depicted in Fig. 3, obtained from the whole set of initial conditions. This distribution is directly comparable with the PST calculations shown in Fig. 8 of Ref. [14]. In fact, application of Eq. (18) in order to ‘add’ a rotational structure to this curve would trivially reduce it to the quantum version of the least-biased/PST distribution. At last, by comparing this with the final theoretical curves, it is readily seen how the suppression observed in the low- $E_t$  part are correctly described by QCT.

It is important to address one last point referring to the insertion of the rotational structures in Section II D. In principle, one might think that a different, simpler approach could be used: To additionally fix all rotational quantum numbers and propagate separate ensembles for each semiclassical state, very much as we have done here for each scissor excitation or can be found elsewhere, *e.g.* [40]. However, with respect to the initial conditions there is a basic difference in the way the vibrational and rotational modes are determined [13]. Using the normal-mode approximation, the former are assigned precise *energies* corresponding to the quantum values. This means that normal mode displacements and conjugate momenta are calculated to exactly match the desired energy in the particular mode. On the other hand, classically, after fixing the *angular momentum vector* for a particular fragment, there remains an indetermination in the rotational energy due to the vibration-rotation coupling. In other words, there are different inertia tensors due to dissimilar normal-mode displacements which will result in different energies even for the same angular momentum. In the case of ketene, for example, calculations after additionally fixing the values of  $j_1$  and  $\kappa_1$  yield broad structures in the correlated translational energy distributions which are several hundred inverse centimetres wide. This would completely blur the rotational structures observed in Fig. 3. The indetermination should be smaller for symmetric tops—where a formula exists that determines the energy in terms of the angular momentum and one of its components—but still would, in general, strongly limit the QCT rotational resolution.



#### IV. SUMMARY AND CONCLUSIONS

A QCT algorithm has been presented that allows to simulate indirect polyatomic processes involving exit-channel effects up to rovibrational resolution without the use of any binning or weighting procedure. It consists of three stages: (1) initial conditions are started in terms of angle-action variables to individually select the experimental states to be studied, which are later transformed into Cartesian coordinates for trajectory integration; (2) trajectories are propagated using an inverse dynamics simulation in the spirit of the exit-channel corrected phase space theory of Hamilton and Brumer; and (3) finally, an approximate quasi-classical formula is used to accurately incorporate possible rotational structures into the quasi-classical product distributions. Of these, only the second step is linked to the statistical assumptions inherent to the study of indirect processes, being the other two of general applicability.

The method was introduced and its capabilities il-

lustrated with the simulation of highly-resolved correlated translational energy distributions from recent experiments in the photo-dissociation of ketene at 308 nm [14]. After slightly modifying the PES to deal with an overestimation of the energy transfer among rotational and translational degrees of freedom, calculated distributions with both vibrational and rotational resolution are in good agreement with the experiment.

#### ACKNOWLEDGEMENTS

Support from an Inter-University Agreement on International Joint Doctorate Supervision between the Instituto Superior de Tecnologías y Ciencias Aplicadas, Cuba and the Université Bordeaux 1, France, as well as the PNCB/2/4 project of the Departamento de Física General in the Cuban institution, are gratefully acknowledged.

- 
- [1] W. H. Miller, *J. Chem. Phys.*, 2006, **125**, 132305.
- [2] R. N. Porter and L. M. Raff, *Dynamics of Molecular Collisions, Part B*, Plenum, New York, 1976.
- [3] D. G. Truhlar and J. T. Muckerman, in *Atom-Molecule Collision Theory: A Guide for the Experimentalist*, Plenum Press, New York, 1979, ch. Reactive Scattering Cross Sections: Quasiclassical and Semiclassical Methods, p. 505.
- [4] T. D. Sewell and D. L. Thompson, *Int. J. Mod. Phys. B*, 1997, **11**, 1067.
- [5] L. Bonnet and J.-C. Rayez, *Chem. Phys. Lett.*, 1997, **227**, 183.
- [6] L. Bañares, F. J. Aoiz, P. Honvault, B. Bussery-Honvault and J. M. Launay, *J. Chem. Phys.*, 2003, **118**, 565.
- [7] L. Bonnet and J.-C. Rayez, *Chem. Phys. Lett.*, 2004, **397**, 106.
- [8] T. Xie, J. M. Bowman, J. W. Duff, M. Braunstein and B. Ramachandran, *J. Chem. Phys.*, 2005, **122**, 014301.
- [9] M. L. González-Martínez, L. Bonnet, P. Larrégaray and J.-C. Rayez, *J. Chem. Phys.*, 2007, **126**, 041102.
- [10] L. Bonnet, *J. Chem. Phys.*, 2008, **128**, 044109.
- [11] M. L. González-Martínez, W. Arbelo-González, J. Rubayo-Soneira, L. Bonnet and J.-C. Rayez, *Chem. Phys. Lett.*, 2008, **463**, 65.
- [12] Z. Sun, D. H. Zhang, C. Xu, S. Zhou, D. Xie, G. Lendvay, S. Y. Lee, S. Y. Lin and H. Guo, *J. Am. Chem. Soc.*, 2008, **130**, 14962.
- [13] M. L. González-Martínez, L. Bonnet, P. Larrégaray, J.-C. Rayez and J. Rubayo-Soneira, *J. Chem. Phys.*, 2009, **130**, 114103.
- [14] A. V. Komissarov, M. P. Minitti, A. G. Suits and G. E. Hall, *J. Chem. Phys.*, 2006, **124**, 014303.
- [15] V. Zabransky and R. W. Carr, Jr., *J. Chem. Phys.*, 1975, **79**, 1618.
- [16] D. J. Nesbitt, H. Petek, M. F. Foltz, S. V. Filseth, D. J. Bamford and C. B. Moore, *J. Chem. Phys.*, 1985, **83**, 223.
- [17] H. Bitto, I.-C. Chen and C. B. Moore, *J. Chem. Phys.*, 1986, **85**, 5101.
- [18] I.-C. Chen, W. H. Green, Jr. and C. B. Moore, *J. Chem. Phys.*, 1988, **89**, 314.
- [19] W. H. Green, Jr., I.-C. Chen and C. B. Moore, *Ber. Bunsenges. Physik. Chem.*, 1988, **84**, 389.
- [20] E. D. Potter, M. Gruebele, L. R. Khundkar and A. H. Zewail, *Chem. Phys. Lett.*, 1989, **164**, 463.
- [21] S. J. Klippenstein and R. A. Marcus, *J. Chem. Phys.*, 1989, **91**, 2280.
- [22] S. K. Kim, Y. S. Choi, C. D. Pibel, Q.-K. Zheng and C. B. Moore, *J. Chem. Phys.*, 1990, **94**, 1954.
- [23] W. H. Green, Jr., A. J. Mahoney, Q.-K. Zheng and C. B. Moore, *J. Chem. Phys.*, 1990, **94**, 1961.
- [24] S. J. Klippenstein and R. A. Marcus, *J. Chem. Phys.*, 1990, **93**, 2418.
- [25] I. Garcia-Moreno, E. R. Lovejoy and C. B. Moore, *J. Chem. Phys.*, 1994, **100**, 8890.
- [26] I. Garcia-Moreno, E. R. Lovejoy and C. B. Moore, *J. Chem. Phys.*, 1994, **100**, 8902.
- [27] C. G. Morgan, M. Drabbels and A. M. Wodtke, *J. Chem. Phys.*, 1996, **104**, 7460.
- [28] C. G. Morgan, M. Drabbels and A. M. Wodtke, *J. Chem. Phys.*, 1996, **105**, 4550.
- [29] S. J. Klippenstein, A. L. L. East and W. D. Allen, *J. Chem. Phys.*, 1996, **105**, 118.
- [30] E. A. Wade, H. Clauberg, S. K. Kim, A. Mellinger and C. B. Moore, *J. Phys. Chem. A*, 1997, **101**, 732.
- [31] E. A. Wade, A. Mellinger, M. A. Hall and C. B. Moore, *J. Phys. Chem. A*, 1997, **101**, 6568.
- [32] M. L. Costen, H. Katayanagi and G. E. Hall, *J. Phys. Chem. A*, 2000, **104**, 10247.
- [33] K. M. Forsythe, S. K. Gray, S. J. Klippenstein and G. E. Hall, *J. Chem. Phys.*, 2001, **115**, 2134.
- [34] J. Liu, F. Wang, H. Wang, B. Jiang and X. Yang, *J. Chem. Phys.*, 2005, **122**, 104309.
- [35] I. Hamilton and P. Brumer, *J. Chem. Phys.*, 1985, **82**,

- 595.
- [36] W. H. Miller, *Adv. Chem. Phys.*, 1974, **25**, 69.
- [37] H. Goldstein, *Classical Mechanics*, Addison-Wesley, MA, 2nd edn., 1980.
- [38] D. M. Wardlaw and R. A. Marcus, *J. Chem. Phys.*, 1985, **83**, 3462.
- [39] M. S. Child, *Semiclassical Mechanics with Molecular Applications*, Clarendon, Oxford, 1991.
- [40] F. J. Aoiz, V. Sáez-Rábanos, T. González-Lezana and D. E. Manolopoulos, *J. Chem. Phys.*, 2007, **126**, 161101.
- [41] A. J. C. Varandas, *Chem. Phys. Lett.*, 1994, **225**, 18.
- [42] P. Larrégaray, L. Bonnet and J.-C. Rayez, *Phys. Chem. Chem. Phys.*, 2002, **4**, 1781.
- [43] R. D. Levine and R. B. Bernstein, *Molecular Reaction Dynamics and Chemical Reactivity*, Oxford University Press, Oxford, 1987.
- [44] R. N. Zare, *Angular Momentum*, Wiley, New York, 1988.
- [45] P. R. Bunker and P. Jensen, *Fundamentals of Molecular Symmetry*, Institute of Physics Publishing, IoP London, 2005.
- [46] H. Petek, D. J. Nesbitt, D. C. Darwin and C. B. Moore, *J. Chem. Phys.*, 1987, **86**, 1172.
- [47] U. Bley and F. Temps, *J. Chem. Phys.*, 1993, **98**, 1058.